Supplementary information for: All-silica nanofluidic devices for DNA-analysis fabricated by imprint of sol-gel silica with silicon stamp

Morten Bo Mikkelsen,[a] Alban A. Letailleur,[b] Elin Søndergård,[b] Etienne Barthel,[b] Jérémie Teisseire,[b] Rodolphe Marie,[a] and Anders Kristensen*[a]

1 Imprint process

Figure 1 shows the surface profile of imprints in sol-gel silica of equal 50 μm wide, 600 nm tall stamp protrusions of silicon and polydimethylsiloxane (PDMS) stamps. The flexibility of PDMS causes a much larger bending of the stamp, compared to a silicon stamp, which leads to a non-planar surface that could not be bonded to a glass lid. A rigid silicon stamp is therefore needed to produce surfaces of the right quality.

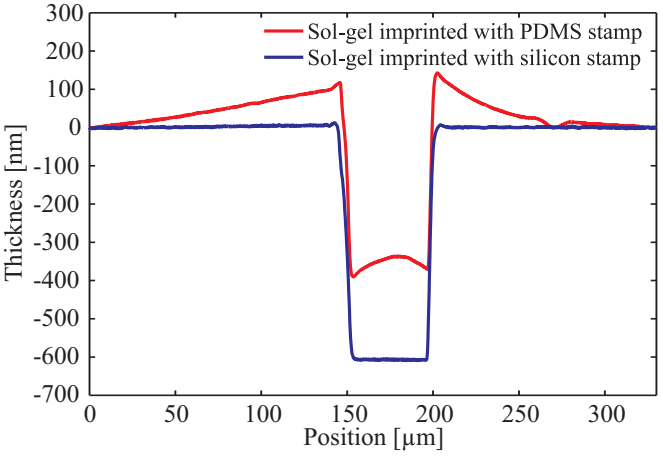

Fig. 1 Imprint of 50 μm wide protrusion with PDMS stamp and silicon stamp.

Imprint of sol-gel silica with a non-permeable stamp is only possible if the water content of the material is reduced before imprint. Imprinting too wet a gel will give defects due to evaporating water and the sol-gel material may stick too the stamp. Surface defects due to evaporating water are shown in Fig. 2a.

However, if the gel is too cured or the water content is too small, viscosity is increased and material flow during imprint is reduced. Furthermore, self-assembly defects, as shown in Fig. 2b, appear.

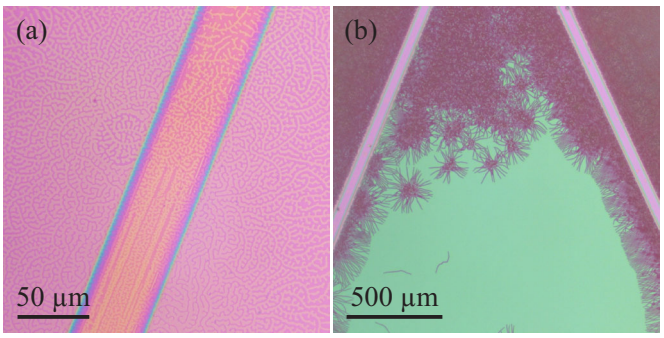

Fig. 2 (a) Too high water content of gel causes one type of surface defects during imprint. (b) Imprinting too cured a gel creates another type of surface defects.

2 Deformation during annealing

For sol-gel thin films, which adhere to a substrate, compressive stress limits the thickness that can be obtained without the film cracking [1].

In an experiment, sol-gel silica films of different thickness were spin-coated on silicon substrates and annealed at 600°C in oxygen atmosphere. Figure 3 shows the final thickness after annealing as function of the initial film thickness. A linear shrinkage to 56% of the initial thickness is found.

The markers in Fig. 3 indicate the film quality after annealing. Circles show that films of initial thickness up to 700 nm are perfectly crack-free. For films of initial thickness between 700 nm and 1 μm, marked by triangles, cracks may occur in the bottom of imprinted structures or around other surface defects that serve as nucleation points, but as the thickness increases, cracks also appear in the middle of large unstructured areas. For films of initial thickness above 1 μm, marked by squares, narrow bands of material peel off and coil up, thereby creating glass wool on the substrate surface, as seen

[a] *DTU Nanotech, Technical University of Denmark, DK-2800 Kongens Lyngby, Denmark. E-mail: anders.kristensen@nanotech.dtu.dk*
[b] *Laboratoire Surface du Verre et Interfaces, Unité Mixte CNRS/Saint-Gobain, 39 quai Lucien Lefranc, F-93303 Aubervilliers Cedex, France. E-mail: elin.sondergard@saint-gobain.com*

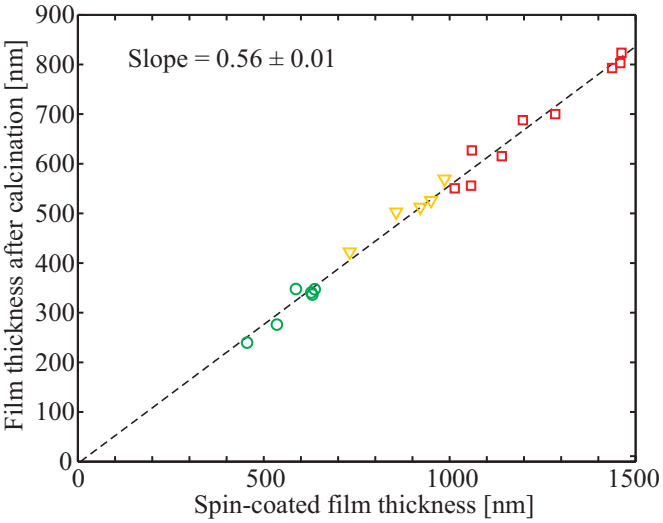

Fig. 3 Thickness of sol-gel silica films on silicon substrates measured after calcination at 600°C as function of the initial spin-coated thickness. A linear reduction of the film thickness to 56% is seen. Circles show crack-free films, triangles show films with few cracks around surface defects and imprinted structures, squares show films that produced glass wool.

in Fig. 4. During the annealing process, the cracking of films start at 400°C and happens during 10 min at 5°C/min temperature ramping. This corresponds well with the fact that calcination of the organics is expected to occur at temperatures above 400°C.

Cracking thus puts a limit to the thickness of sol-gel silica thin films of approximately 700 nm, corresponding to 400 nm final thickness. For sol-gel materials which are not clamped to a substrate, much larger items can be manufactured, since the free surfaces can accommodate for the shrinkage without introducing stress. An example of this is casting of bulk gels[2].

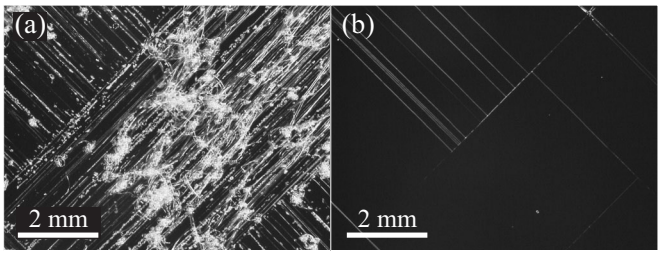

Fig. 4 Optical microscope images of calcinated sol-gel silica films of (a) 2 μm initial thickness and (b) 1 μm initial thickness. In (a), narrow bands of material peel off, following the ⟨100⟩-directions of the silicon substrate, and coil up, creating glass wool on the surface. In (b), cracks occur along the same directions, but the material does not peel off. Image bottom lines are parallel to the substrate flats, *i.e.* the ⟨110⟩-direction.

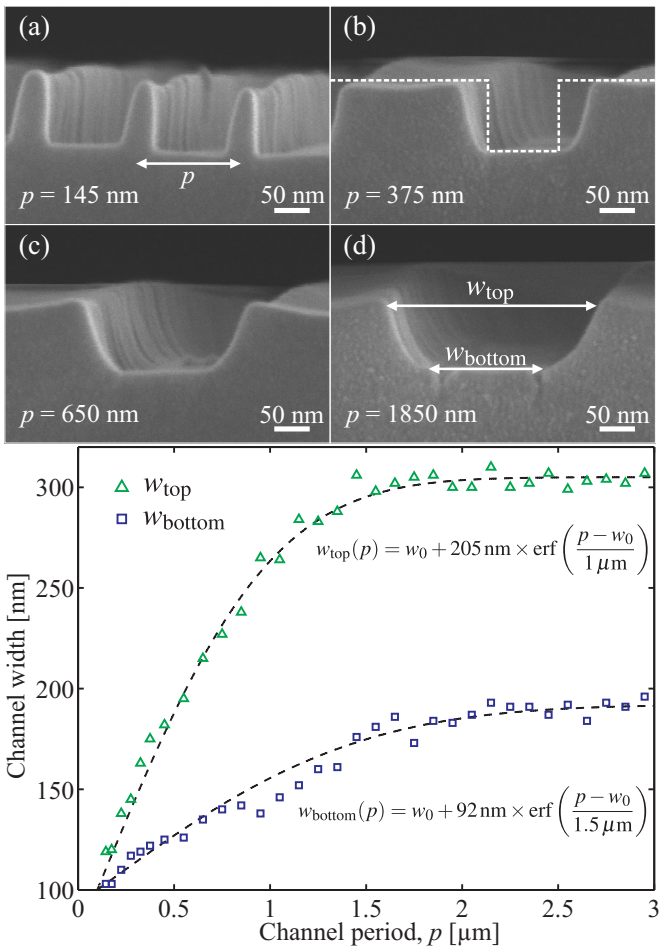

Fig. 5 SEM images (a-d) show cross-sectional views of calcinated imprints of $w_0 = 100$ nm wide, $h_0 = 100$ nm deep structures with increasing period p from (a) through (d). Dashed line in (b) shows cross-sectional profile of the stamp structure for comparison. The width of imprinted channels is seen to depend strongly on the period due to the deformation of sol-gel silica that takes place during the annealing process. The graph shows values of w_{top} and w_{bottom}, measured on the SEM images, as indicated in (d). The data are excellently fitted by the inserted error functions, which are shown with dashed lines.

Cracking of sol-gel silica films occurs equally frequent on silicon and fused silica substrates. However, where cracks on the amorphous fused silica substrate follow random paths, cracks on a (100) silicon substrate follows the ⟨100⟩ crystal directions, *i.e.* at a 45° angle to the primary flat, as seen in Fig. 4. This may be caused by an interplay between the anisotropic Young's modulus of silicon[3], $E_{\langle 110\rangle} = 169$ GPa and $E_{\langle 100\rangle} = 130$ GPa, and the isotropic coefficient of thermal expansion[4].

In the regions around imprinted channel structures, the deformation is more complex. Away from the surface structures,

all in-plane forces balance each other, and deformation only happens in the direction normal to the free surface. When channels are imprinted, vertical free surfaces are introduced, which will be deformed due to the compressive stress. However, at the bottom of the channel, less deformation is possible than at the top of the channel. The deformation depends on the free-surface density and hence on the amount of material next to the channel. This is shown in Fig. 5, where 100 nm wide, 100 nm deep channels with a period increasing from 145 nm to 3 μm were imprinted in a 700 nm sol-gel silica film and the resulting channel dimensions measured after annealing.

In Fig. 5a, the 100 nm wide channel imprinted at 145 nm average period has bottom width of 100 nm and top width of 115 nm. Next to it, a 25–40 nm wide, 95 nm tall, protruding line is seen, which was imprinted by a stamp cavity designed to be 40 nm by 100 nm. A high degree of dimensional control is thus possible for structures of small period, and nearly vertical side walls of the imprinted channels are obtained. For structures of large period, the deformation is much more pronounced: in Fig. 5d, the same 100 nm channel imprinted at 1850 nm period has bottom width of 166 nm and top width of 299 nm.

The bottom panel of Fig. 5 shows the channel widths measured at top and bottom as function of the period. It is seen that the data are excellently fitted by error functions, as shown by the dashed lines in the graph.

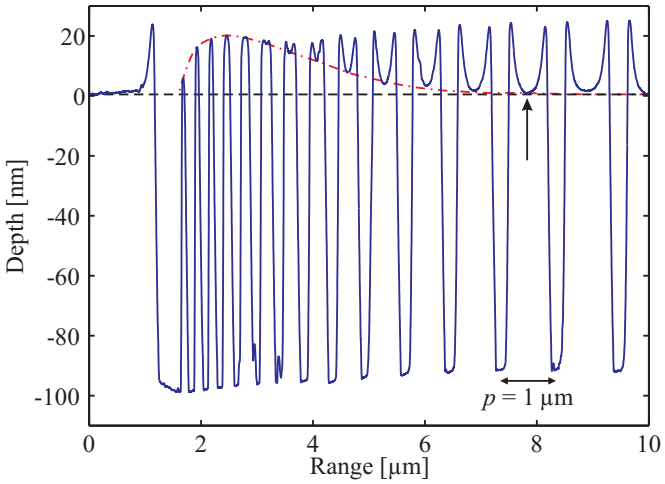

Fig. 6 AFM surface profile of the structures in Fig. 5. Horizontal dashed line indicates the surface level of the unstructured bulk areas of the film. Dash-dotted line shows the level of the centers of the protruding structures separating the channels. For periods $p > 1\,\mu$m, corresponding to a structure widths larger than 900 nm, the level of the center of the structures reach the bulk surface level, as indicated by the arrow. Hence, for $p > 1\,\mu$m, the structure deformation is independent of p, since the deformation of the edges only influences the outer approximately 450 nm of the material.

Figure 6 shows the surface profile, made by atomic force microscopy (AFM), of the same structures as in Fig. 5. It is seen that for periods $p > 1\,\mu$m, corresponding to channel separations larger than 900 nm, the center levels of the protruding structures reach the bulk surface level. Hence, for $p > 1\,\mu$m, the structure deformation is independent of p, since the deformation of the edges only influences the outer approximately 450 nm of the material. This corresponds to the 1 μm constant in the fit of $w_{\mathrm{top}}(p)$.

3 Device fabrication

Figure 7 shows cross-sectional sketches of the process flow for fabrication of imprinted nanofluidic sol-gel silica devices. Channels of different depths are defined in the spin-coated gel film by imprinting of a multi-level hybrid stamp. Microprotrusions on the stamp are made by UV-lithography of Ormo-Comp and nanoprotrusions are made by electron lithography and reactive-ion etching of thermally grown silicon dioxide[6].

After demolding and annealing of the the imprinted sol-gel silica, the nanofluidic device is assembled in the same manner as devices fabricated by reactive-ion etching:[7–9] Powder blasting[10] through a masking tape is used for making inlet holes, and fusion bonding[11] is used to seal the channels by bonding of a polished cover slip to the imprinted sol-gel silica surface.

References

1 C. J. Brinker and G. W. Scherer, *Sol-Gel Science: The Physics and Chemistry of Sol-Gel Processing*, Academic Press, San Diego, CA, 1990.
2 T. Kreuzberger, A. Harnisch, M. Helgert, L. Erdmann and R. Brunner, *Microelectronic Engineering*, 2009, **86**, 1173 – 1175.
3 J. J. Wortman and R. A. Evans, *Journal of Applied Physics*, 1965, **36**, 153–156.
4 R. B. Roberts, *Journal of Physics D: Applied Physics*, 1981, **14**, L163.
5 M. Born and E. Wolf, *Principles of Optics: Electromagnetic Theory of Propagation, Interference and Diffraction of Light*, Cambridge University Press, Cambridge, UK, 7th edn., 2005.
6 L. H. Thamdrup, A. Klukowska and A. Kristensen, *Nanotechnology*, 2008, **19**, 125301.
7 J. O. Tegenfeldt, C. Prinz, H. Cao, S. Chou, W. W. Reisner, R. Riehn, Y. M. Wang, E. C. Cox, J. C. Sturm, P. Silberzan and R. H. Austin, *Proceedings of the National Academy of Sciences of the United States of America*, 2004, **101**, 10979–10983.
8 F. Persson, P. Utko, W. Reisner, N. B. Larsen and A. Kristensen, *Nano Letters*, 2009, **9**, 1382–1385.
9 M. B. Mikkelsen, W. Reisner, H. Flyvbjerg and A. Kristensen, *Nano Letters*, 2011, **11**, 1598–1602.
10 F. Persson, L. H. Thamdrup, M. B. L. Mikkelsen, S. E. Jarlgaard, P. Skafte-Pedersen, H. Bruus and A. Kristensen, *Nanotechnology*, 2007, **18**, 245301.
11 A. Plößl and G. Kräuter, *Materials Science and Engineering: R: Reports*, 1999, **25**, 1–88.

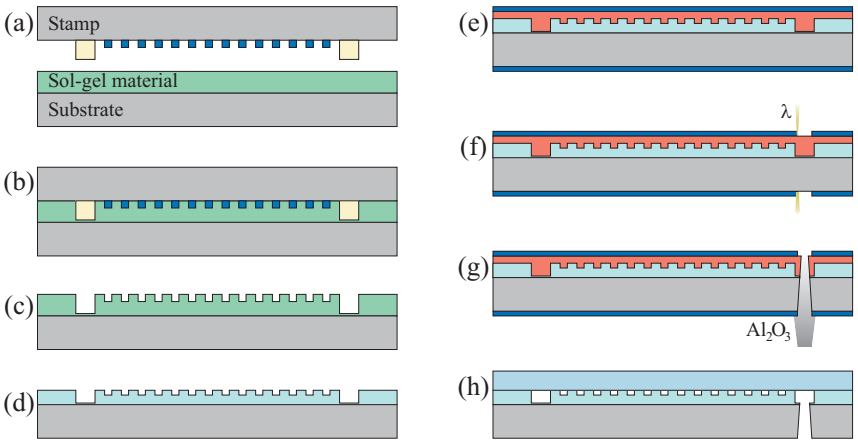

Fig. 7 Cross-sectional sketches of the process flow. (a) Imprint of multi-level hybrid stamp in spin-coated gel film. (b) Heating during imprint to cross-link the gel material. (c) Demolding of stamp. (d) Thermal annealing of gel at 600°C in oxygen atmosphere calcinates organics and produces pure silica. (e) Spin-coating of protective resist layer (red) and application of self-adhesive masking tape (blue, Nitto SWT-20). (f) Laser marking of tape using CO_2-laser ($\lambda = 10.6\,\mu$m). Silicon substrates are transparent at this wavelength, enabling simultaneous marking of both sides. (g) Powder blasting of inlet holes through the masking tape using 110 μm Al_2O_3 particles. (h) Sealing of fluidic channels by fusion bonding of a polished 157 μm thick cover slip to the imprinted sol-gel silica surface. Subsequent thermal annealing at 550°C strengthens the bond.